Weak gravitational deflection by two-power-law densities using the Gauss-Bonnet theorem

Karlo de Leon* and Ian Vega†

National Institute of Physics, University of the Philippines, Diliman, Quezon City, 1101, Philippines

(Received 23 March 2019; published 10 June 2019)

We study the weak deflection of light by nonrelativistic mass distributions described by two-power-law densities $\rho(R) = \rho_0 R^{-\alpha}(R+1)^{\beta-\alpha}$, where α and β are non-negative integers. New analytic expressions of deflection angles are obtained via the application of the Gauss-Bonnet theorem to a chosen surface on the optical manifold. Some of the well-known models of this two-power-law form are the Navarro-Frenk-White (NFW) model $(\alpha,\beta) = (1,3)$, Hernquist (1,4), Jaffe (2,4), and the singular isothermal sphere (2,2). The calculated deflection angles for Hernquist and NFW agree with that of Keeton and Bartelmann, respectively. The limiting values of these deflection angles (at zero or infinite impact parameter) are either vanishing or similar to the deflection due to a singular isothermal sphere. We show that these behaviors can be attributed to the topological properties of the optical manifold, thus extending the pioneering insight of Werner and Gibbons to a broader class of mass densities.

DOI: 10.1103/PhysRevD.99.124007

I. INTRODUCTION

Gravitational lensing has come a long way since its entry to modern science. Eddington's famous expedition to capture light deflection from the solar eclipse of 1919 is generally recognized as the first to provide general relativity its sound empirical grounding [1,2]. In the years since, the bond between lensing and general relativity has only strengthened, aided by increasingly more sophisticated instruments and techniques [3,4]. In the process, gravitational lensing has slowly outgrown its status as a mere theoretical prediction. It is now an indispensable tool for much of modern astrophysics and cosmology, serving as a primary probe for characterizing mass distributions throughout the cosmos [5–12], particularly in the high redshift regime [13–18].

This paper returns to lensing's classic roots, by focusing on the relation between the lensing behavior of a galaxy and its mass distribution. A lens model is an important initial assumption in inverting lensed images back to its source image [19,20]. In astrophysics, knowing the expected lensing behavior of a density model is essential in testing its applicability for modeling mass clusters. Generally, the lensing properties of a density function, such as the deflection angle and magnification, are not readily solvable. Mass models are then typically chosen based on how readily observables can be calculated from them.

Many of the commonly used density functions for galaxies and dark matter halos belong to the family of density parametrizations whose generalized form first appeared in a paper by Hernquist [21],

$$\rho(R) = \frac{\rho_0}{R^{\alpha}(R^{1/\gamma}+1)^{(\beta-\alpha)\gamma}}, \tag{1}$$

where $R = r/r_0$. This has become a common choice for modeling due to its relatively simple form and its analytic properties [22–24]. Here, there are two scale parameters r_0 and ρ_0, and three exponential parameters (α,β,γ) that modify the general shape of the distribution. Central growth is controlled by α: $\rho \sim R^{-\alpha}$ for small R. This takes into account the central cusp observed on the surface brightness profiles of some galaxies, even at high resolution imaging [25–27]. The allowed divergence is restricted to values $\alpha < 3$, so that the mass function (10) may still be defined. Meanwhile, radial decay is regulated by β: $\rho \sim R^{-\beta}$ for large R. Physically relevant distributions decay no slower than $1/r^2$, so we limit our discussion to the range $\beta \geq 2$. The density profile (1) is a function that provides a smooth transition between these two power laws, with the exponent γ measuring the width of the transition region.

Here, we study the weak gravitational deflection of the so-called two-power-law densities, the $\gamma = 1$ subset of the Hernquist family,

$$\rho(R) = \frac{\rho_0}{R^{\alpha}(R+1)^{\beta-\alpha}}. \tag{2}$$

In particular, we calculate the deflection angle in the high-frequency and weak-field limit, with the source and observer both at spatial infinity. It turns out that for integer

*kndeleon@nip.upd.edu.ph
†ivega@nip.upd.edu.ph

values of α and β, the deflection angle can be expressed analytically, and so we limit our discussion to these values. Models belonging to this set include the famous Navarro-Frenk-White (NFW) model $(\alpha,\beta)=(1,3)$, Hernquist (1,4), Jaffe (2,4), and the singular isothermal sphere (2,2) [21,28,29]. Previous calculations have worked out deflection angles arising from densities related to this form, but with significant restrictions, such as on the $(\alpha,\beta,1/2)$ subset that closely resembles the two-power law [30,31], a much restricted range of the two-power law [32], and on individual values of α and β [33]. Evans and Wilkinson [34] have also studied two-power-law forms similar to Eq. (2), but for the projected surface mass density rather than the three-dimensional density we use here.

Our calculation utilizes the Gauss-Bonnet method by Gibbons and Werner [35], which nicely highlights the often overlooked role of topology in gravitational lensing. This seminal work motivated us to understand the extent to which the topological arguments made by [35] generalize to a much broader class of density functions. Our results shall show that, indeed, gross features of weak deflection are due to topological properties of an underlying *optical manifold*. Beyond this question of principle, we also argue that for weak deflection of (at least) spherically symmetric distributions, the Gauss-Bonnet approach holds a number of advantages over common methods such as the thin-lens approximation and direct calculations based on metric components. (We shall say more about this in Sec. IV.) Previous works have exploited these advantages to study weak deflection in various contexts [36–38]. Though curiously, almost none of the extant literature applies to model density functions that are particularly useful for astrophysical work. Our work partly seeks to rectify this state of affairs.

The rest of this paper proceeds as follows: first, we go over some preliminaries, particularly the Gauss-Bonnet theorem based on the optical metric, and a short summary of Gibbons and Werner's method. New expressions for the deflection angles of the densities are then derived, and this is followed by a discussion of general observations and comparisons. This brings to the fore the perspective advocated by Gibbons and Werner that gross physical features of weak deflection are primarily determined by the topology and geometry of the underlying optical manifold. The examples we explicitly work out all lend further credence to this point of view. Finally, the paper concludes with a summary and recommendations for future work.

We will use the signature $(-,+,+,+)$ and geometric units wherein $c=G=1$ throughout.

II. GAUSS-BONNET THEOREM

In the Gibbons-Werner approach to the weak gravitational deflection of light, the deflection angle is directly calculated from the well-known Gauss-Bonnet theorem of classical differential geometry. The theorem has made many appearances in various fields of physics. (See e.g., [39–44], just to name a few.) For completeness, we briefly review this here.

Let M be a compact, oriented (and thus, triangularizable) surface with a piecewise-smooth boundary ∂M, where the curve is arclength-parametrized and traversed in the positive sense. The Gauss-Bonnet theorem then states that

$$\iint_M K dS + \int_{\partial M} \kappa dt + \sum_i \alpha_i = 2\pi\chi(M), \tag{3}$$

where t is the arclength parameter, α_i are the external angles at the vertices of ∂M, K is the Gaussian curvature, κ is the geodesic curvature, and χ is the Euler characteristic of M (e.g., [45], p. 139). The geodesic curvature of a smooth curve γ on a surface with metric g, with unit tangent vector $\dot{\gamma}$, and unit acceleration vector $\ddot{\gamma}$, is defined as

$$\kappa = g(\nabla_{\dot{\gamma}}\dot{\gamma},\ddot{\gamma}), \tag{4}$$

while the Gaussian curvature is proportional to the single nontrivial component of the Riemann curvature tensor for two dimensions (Gauss's Theorema Egregium):

$$K = R_{1212}/|g| \tag{5}$$

with $|g|$ the determinant of the metric [45][pp. 64, 78].

The theorem is applied to a choice of surface D defined on the optical metric space, which then generates an expression involving the deflection angle.

III. OPTICAL METRIC

The metric of a static and spherically symmetric spacetime has the general form

$$ds^2 = -e^{2A(r)}dt^2 + e^{2B(r)}dr^2 + r^2(d\theta^2 + \sin^2\theta d\phi^2). \tag{6}$$

Spherical symmetry guarantees that geodesics lie on a plane and are equivalent up to spatial rotations about the origin. Thus, we can set any geodesic to lie on the equatorial plane $\theta=\pi/2$, without loss of generality. Working only with null paths allows us to further reduce the number of dimensions by considering another manifold with the spacelike coordinate t defined as the new interval. From the metric $g_{\mu\nu}$ (6), we consider the conformal transformation $\tilde{g}_{\mu\nu}=g_{\mu\nu}/g_{00}$. With this metric, we set $ds^2=0$, and define t as the new interval,

$$dt^2 = g^{\text{opt}}_{ab}dx^a dx^b = e^{2(B(r)-A(r))}dr^2 + e^{-2A(r)}r^2 d\phi^2. \tag{7}$$

This is the optical metric $g^{\text{opt}}_{ab}=g_{ab}/(-g_{00})$. While geodesics in general are not preserved under conformal transformations, it does hold for null curves (e.g., [46], p. 446).

So, light paths are still faithfully represented by geodesic curves.

For the perfect fluid case, the energy-momentum tensor is $T^{\mu\nu} = \mathrm{diag}(\rho, p, p, p)$ in the rest frame of the fluid, where ρ is the energy density and p is the isotropic rest-frame pressure. Plugging this into Einstein's field equations, the metric components are to be determined from the energy-momentum tensor components as

$$\frac{dA}{dr} = \left(1 - \frac{2m(r)}{r}\right)^{-1}\left(\frac{m(r)}{r^2} + 4\pi G r p\right), \tag{8}$$

$$e^{-2B(r)} = 1 - \frac{2m(r)}{r}, \tag{9}$$

where $m(r)$ is the mass function

$$m(r) \coloneqq \int_0^r \rho(r')4\pi r'^2 dr' \tag{10}$$

(e.g., [47], pp. 261 and 262). With the specification of an equation of state or, in our case, a density function, the pressure can be calculated from the Tolman-Oppenheimer-Volkoff equation

$$\frac{dp}{dr} = -\frac{(\rho + p)(m + 4\pi r^3 p)}{r^2(1 - 2(m/r))}, \tag{11}$$

derived from the Einstein field equations and the conservation of energy-momentum tensor, which is also a consequence of the former [[47] p. 264]. These equations, plus boundary conditions, completely define the metric due to the perfect fluid.

In terms of the physical parameters of the density function in Eq. (2), the nonrelativistic limit is taken to be the low-density case $\mu \coloneqq \rho_0 r_0^2 \ll 1$, keeping terms only linear in μ. Pressure contributions may be neglected in this limit. To see this, we nondimensionalize the quantities in Eq. (11). Let $\tilde{\rho} \coloneqq \rho r_0^2$, $\tilde{p} \coloneqq p r_0^2$, $\tilde{m} \coloneqq m/r_0$, and again $R = r/r_0$. We then have

$$\frac{d\tilde{p}}{dR} = -\frac{(\tilde{\rho} + \tilde{p})(\tilde{m}/R + 4\pi R^2 \tilde{p})}{R(1 - 2(\tilde{m}/R))}. \tag{12}$$

Note that both $\tilde{\rho}$ and $\tilde{m}$ are proportional to μ. Next, we assume an expansion of $\tilde{p}$ in powers of μ, that is, we write $\tilde{p} = a_0 + a_1\mu + \mathcal{O}(\mu^2)$. But since the pressure of a vacuum is zero, $a_0 = 0$. Thus up to first order, we find that $\tilde{p}$ is also proportional to μ. Now, the right-hand side of Eq. (12) is at least of $\mathcal{O}(\mu^2)$, so $d\tilde{p}/dR = 0$ at first order, implying that the pressure is constant at this limit. The pressure is expected to vanish at spatial infinity, and so it must vanish everywhere.

IV. SURFACE CONSTRUCTION

Here we give a short review of the surface designed by Gibbons and Werner [35] for calculating deflection angles through the Gauss-Bonnet theorem. Note, however, that such surface constructions are not unique (e.g., [48,49]).

On the optical manifold, let the origin of the coordinate system (r, ϕ) be at the center C of the mass distribution (see Fig. 1). The geodesic curve Γ is the trajectory of the photon emitted at the source S with impact parameter b and received by an observer at O. Further, let S and O be at an equal distance d from C. The angle δ between the tangent of Γ at O and the line $\phi = \pi$ is the deflection angle δ. We take the limit $d \to \infty$ so that S and O are at spatial infinity, and $\phi(S) = 0$ and $\phi(O) = \pi + \delta$. Now, we construct a surface from Γ by considering an additional circular arc γ centered at C, intersecting Γ at points S and O. Let D be this surface bounded by Γ and γ.

The Gauss-Bonnet theorem on surface D reads

$$\int_0^{\pi+\delta}\int_{(r\circ\Gamma)(\phi)}^{\infty} K\sqrt{|g^{\mathrm{opt}}|}\,dr\,d\phi + \int_0^{\pi+\delta}\left(\kappa\frac{dt}{d\phi}\right)d\phi + \left(\frac{\pi}{2} + \frac{\pi}{2}\right) = 2\pi, \tag{13}$$

noting that the differential element dS in coordinate form is

$$dS = \sqrt{|g^{\mathrm{opt}}|}\,dr\,d\phi, \tag{14}$$

and the external angles at S and O are $\pi/2$. The surface D does not contain the possibly singular point C, so the surface is simply connected and has an Euler characteristic $\chi = 1$. The Gaussian curvature can be computed from Eq. (5) given the metric g^{opt},

$$-K\sqrt{|g^{\mathrm{opt}}|} = \frac{2m}{r^2}\left(1 - \frac{2m}{r}\right)^{-3/2} \times \left(1 - \frac{3m}{2r} - \frac{4\pi\rho r^3}{m}\left(1 - \frac{2m}{r}\right)\right). \tag{15}$$

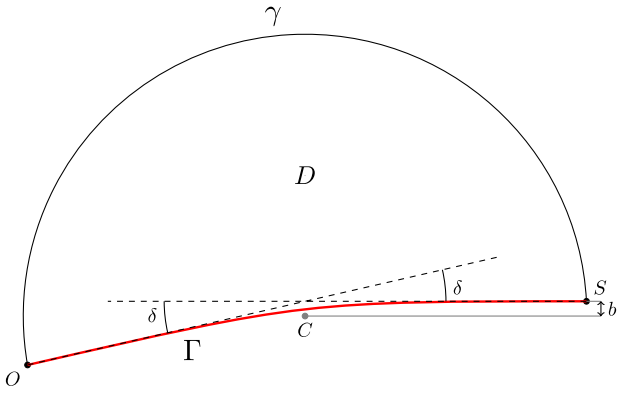

FIG. 1. Surface on the optical manifold used for computing the deflection angle.

In the nonrelativistic limit, Eq. (15) is calculated only up to first order in μ. It then suffices to take only the zeroth order of the geodesic curve $(r\circ\Gamma)(\phi) = b/\sin\phi$ (the undeflected light curve in Minkowski space), and the zeroth order of the angular bound: $\pi + \delta \approx \pi$ [we know that $\delta = 0$ in vacuum, so δ must be at least of order $\mathcal{O}(\mu)$]. With this, we obtain the central equation for calculating deflection angles

$$\int_0^{\pi+\delta}\left(\kappa\frac{dt}{d\phi}\right)d\phi - \pi = \int_0^{\pi}\int_{B/\sin\phi}^{\infty}\mathcal{K}\,dR\,d\phi, \tag{16}$$

where $B = b/r_0$ and $\mathcal{K}$ is the first order in μ of $-Kr_0\sqrt{|g^{\text{opt}}|}$ in Eq. (15),

$$\mathcal{K} \coloneqq \frac{2}{R^2}\frac{m}{r_0} - 8\pi R r_0^2\rho. \tag{17}$$

It is this form $\mathcal{K}$, rather than K, that is directly useful for our calculations. We will call $\mathcal{K}$ the Gaussian curvature *term*.

This method offers a number of advantages in calculating deflection angles from spherical matter distributions compared to canonical methods. Integration from $g(p^\mu, p^\mu) = 0$ (e.g., [47], pp. 283 and 284), where p^μ is the four-momentum of the photon, requires the analytic form of the spacetime metric components. While g_{rr} (of the four-dimensional metric) is readily obtained from the mass function, g_{tt} will have to be computed from Eq. (8), for which an analytic form may not exist. The method of thin-lens approximation partially resolves this problem, since it only requires the energy density function (e.g., [50], p. 25). The difficulty, however, is translated to computing the surface mass density, which is the projection of the mass distribution on a plane orthogonal to the light ray direction $\Sigma = \int \rho \mathrm{d}z$ (with the photon traveling parallel to the z axis). Because the spherical energy density is a function of $r = \sqrt{x^2+y^2+z^2}$, the integrand $\rho\circ r$ can easily have a complicated form in z, even for fairly simple functions $\rho(r)$. In the Gauss-Bonnet method, the central equations (16) and (17) only require the explicit forms of the density and mass function, and the integration is carried out in the r-θ space. For some spacetimes, g_{tt} must still be calculated. But, only the $r \to \infty$ limit is needed, so Eq. (8) further simplifies.

Aside from advantages in calculation, the method also gives insight to the role of the topology in gravitational deflection, as we will see later.

V. CALCULATION OF DEFLECTION ANGLES

As a concrete demonstration of the usefulness of the Gauss-Bonnet method, we now apply this to the two-power density function of Eq. (2). We present the deflection angles in decreasing order of α, and then in decreasing values of β. A general expression of the deflection angle that covers all values of α, β was not obtained due to the discontinuity of the function $f(x,a) = \int^x y^a dy$ at $a = -1$. The calculation splits into separate cases whenever a $\int^x y^{-1}dy$ integration occurs. Most of the calculations are similar and involve only the same family of integrals. The only significant difference is between the cases $\beta > 2$ and $\beta = 2$. Densities with $\beta > 2$ are asymptotically Euclidean, while $\beta = 2$ approaches the singular isothermal distribution at infinity. Before proceeding, we first present three integrals that repeatedly appear in our calculations:

$$\begin{aligned} I_1^q &\coloneqq \int_0^{\pi}\frac{\sin\phi d\phi}{(1+B\csc\phi)^q} \\ &= \frac{1}{B^q}\frac{(-1)^{q-1}}{(q-1)!}\left(\frac{\partial}{\partial a}\right)^{q-1}_{a=1/B} \\ &\quad\times\left(\frac{2}{a} - \frac{\pi}{a^2}\left(1-\frac{1}{\sqrt{1-a^2}}\right) - \frac{2\arcsin a}{a^2\sqrt{1-a^2}}\right), \end{aligned} \tag{18}$$

$$\begin{aligned} I_2^q &\coloneqq \int_0^{\pi}\frac{d\phi}{(1+B\csc\phi)^q} \\ &= \frac{1}{B^q}\frac{(-1)^{q-1}}{(q-1)!}\left(\frac{\partial}{\partial a}\right)^{q-1}_{a=1/B} \\ &\quad\times\left(\frac{\pi}{a}\left(1-\frac{1}{\sqrt{1-a^2}}\right) + \frac{2\arcsin a}{a\sqrt{1-a^2}}\right), \end{aligned} \tag{19}$$

$$\begin{aligned} I_3 &\coloneqq \int_0^{\pi}\sin\phi\ln(1+B\csc\phi)d\phi \\ &= \pi B + 2\ln\frac{B}{2} - 2\sqrt{B^2-1}\arctan\sqrt{B^2-1}. \end{aligned} \tag{20}$$

We will derive these in Appendix B.

A. Case (2, $\beta \geq 4$)

For an asymptotically Euclidean metric, the deflection angle is solely due to the area integral in Eq. (16),

$$\delta = \int_0^{\pi}\int_{B/\sin\phi}^{\infty}\mathcal{K}dRd\phi, \tag{21}$$

since in flat space the geodesic curvature κ of a circular arc is the usual inverse of the radius $\kappa = 1/d$, and $dt/d\phi = d$. The energy density and mass function are

$$\rho(R) = \frac{\rho_0}{R^2(R+1)^{\beta-2}}, \tag{22}$$

$$m(R) = \frac{4\pi\rho_0 r_0^3}{\beta-3}\left(1-\frac{1}{(R+1)^{\beta-3}}\right). \tag{23}$$

Therefore, the Gaussian curvature term gives

$$\mathcal{K} = 8\pi\rho_0 r_0^2\left(\frac{1}{\beta-3}\frac{1}{R^2} - \frac{1}{\beta-3}\frac{1}{R^2(R+1)^{\beta-3}} - \frac{1}{R(R+1)^{\beta-2}}\right). \tag{24}$$

However, this form of $\mathcal{K}$ is not fit for the R-integration. Our workaround is to perform partial fraction decomposition. In the Appendix, we present a general decomposition of the fraction $(R-a)^{-p}(R-b)^{-q}$. The following identities are used to decompose fractions in Eq. (24):

$$\frac{1}{R(R+1)^j} = \frac{1}{R} - \sum_{i=1}^{j} \frac{1}{(R+1)^i}, \tag{25}$$

$$\frac{1}{R^2(R+1)^j} = -\frac{j}{R} + \frac{1}{R^2} + \sum_{i=1}^{j} \frac{j+1-i}{(R+1)^i}. \tag{26}$$

With these, we proceed with the integration and find the deflection angle to be

$$\begin{aligned}\delta(B) &= \frac{8\pi\rho_0 r_0^2}{\beta-3}\int_0^{\pi}\left(\sum_{i=1}^{\beta-3}\frac{1}{(1+B\csc\phi)^i}\right)d\phi \\ &= \frac{8\pi\rho_0 r_0^2}{\beta-3}\left(\frac{2}{B} - \frac{I_1^{\beta-3}}{B}\right).\end{aligned} \tag{27}$$

The summation in Eq. (27) is just a finite geometric sum. It is apparent from this form that $\delta(0) = 8\pi^2\rho_0 r_0^2$ and $\delta(\infty) = 0$. This curious nonvanishing deflection at $B = 0$ (i.e., zero impact parameter) is discussed in Sec. VI. For the Jaffe model (2,4), the deflection angle is simply

$$\delta_{\text{Jaffe}}(B) = 8\pi\rho_0 r_0^2\left(\pi - \frac{2B}{\sqrt{B^2-1}}\operatorname{arcsec} B\right). \tag{28}$$

Deflection angles for a fairly general subset of $(\alpha, \beta, 1)$ densities written in terms of analytic functions, such as Eq. (27), do not exist elsewhere in other literature, as far as we can know. In checking the validity of our expressions, we inspect the limiting values at $B \to 0$ and $B \to \infty$ and analyze their corresponding implications.

B. Case (2,3)

The mass functions of these distributions diverge at spatial infinity, but the deflection angle is still well-behaved. These densities are still asymptotically Euclidean, and the deflection angle is calculated again from Eq. (21). The procedure is similar to the previous case, so we only present the results here:

$$\rho(R) = \frac{\rho_0}{R^2(R+1)}, \tag{29}$$

$$m(R) = 4\pi\rho_0 r_0^3 \ln(R+1), \tag{30}$$

$$\delta(B) = 8\pi\rho r_0^2 \frac{I_3}{B}. \tag{31}$$

Similar to the previous case, $\delta(0) = 8\pi^2\rho_0 r_0^2$ and $\delta(\infty) = 0$.

C. Case (1, $\beta \geq 4$)

We start from Eq. (21) with the following density and mass function:

$$\rho(R) = \frac{\rho_0}{R(R+1)^{\beta-1}}, \tag{32}$$

$$\begin{aligned}m(R) = 4\pi\rho_0 r_0^3\Bigg(&\frac{1}{(\beta-2)(\beta-3)} - \frac{1}{\beta-3}\frac{1}{(R+1)^{\beta-3}} \\ &+ \frac{1}{\beta-2}\frac{1}{(R+1)^{\beta-2}}\Bigg).\end{aligned} \tag{33}$$

The Gaussian curvature term can be written as

$$\mathcal{K} = 8\pi\rho_0 r_0^2\left(-\frac{1}{(R+1)^{\beta-1}} + \frac{1}{(\beta-3)(\beta-2)}\sum_{i=2}^{\beta-2}\frac{i-1}{(R+1)^i}\right), \tag{34}$$

again using the relations (25) and (26). Proceeding further, the deflection angle is

$$\delta(B) = \frac{8\pi\rho_0 r_0^2}{(\beta-2)(\beta-3)}\left(\frac{2}{B} - \frac{I_1^{\beta-2}}{B} - (\beta-2)I_2^{\beta-2}\right), \tag{35}$$

where $\delta(0) = \delta(\infty) = 0$. Thus, the deflection angle of the Hernquist model (1,4) is

$$\delta_{\text{Hern}}(B) = \frac{8\pi\rho_0 r_0^2 B}{B^2-1}\left(1 - \frac{\operatorname{arcsec} b}{\sqrt{B^2-1}}\right). \tag{36}$$

This is consistent with the result presented in the catalog of Keeton [32]. The author used the *scaled* deflection angle so there is a difference in the overall factor of the expression (e.g., [51], p. 158).

D. Case (1,3) (NFW)

Similar to the density (2,3), the mass function of NFW diverges at infinity. The deflection angle can still be calculated, however. The density and mass function of NFW are given by

$$\rho(R) = \frac{\rho_0}{R(R+1)^2}, \tag{37}$$

$$m(R) = 4\pi\rho_0 r_0^3\left(\ln(R+1) - \frac{R}{R+1}\right). \tag{38}$$

Evaluating Eq. (21) yields

$$\delta_{\mathrm{NFW}}(B) = 8\pi\rho_0 r_0^2\left(\frac{I_3}{B} - I_2^1\right) = \frac{16\pi\rho_0 r_0^2}{B}\left(\ln\frac{B}{2} + \frac{1}{\sqrt{B^2-1}}\arctan\sqrt{B^2-1}\right). \tag{39}$$

The deflection angle is defined for all B and has the same limits as the previous case: $\delta(0) = \delta(\infty) = 0$. This expression is equivalent to that of Bartelmann, again up to a factor since the author used the scaled deflection angle [33].

E. Case (1,2)

Densities with $\beta = 2$ have divergent mass functions at infinity and are not asymptotically Euclidean. Unlike the previous cases where the deflection angle is only due to the area integral, here we have a contribution from the circular arc γ. We return to Eq. (16) dealing first with the area integration, then the line integral part.

Evaluating the area integral proceeds similarly:

$$\rho = \frac{\rho_0}{R(R+1)}, \tag{40}$$

$$m(R) = 4\pi\rho_0 r_0^3(R - \ln(R+1)), \tag{41}$$

$$\delta_{\mathrm{area}}(B) = -8\pi\rho r_0^2\frac{I_3}{B}. \tag{42}$$

Now, we compute the metric coefficients to evaluate the line integral. With the given density and mass function, Eqs. (40) and (41), Eqs. (8) and (9) are calculated up to first order in μ giving

$$e^{2A} \approx C^{-2}(R+1)^{8\pi\rho_0 r_0^2(1+R^{-1})}, \tag{43}$$

$$e^{2B} \approx (1 + 8\pi\rho_0 r_0^2) - 8\pi\rho_0 r_0^2\frac{\ln(R+1)}{R}, \tag{44}$$

for some constant C.

The definition of the geodesic curvature (4) involves the covariant derivative operator ∇. For the circular arc, it turns out we do not need all the connection coefficients Γ^i_{jk} to calculate the geodesic curvature. The unit tangent and unit acceleration vector of the circular arc γ are

$$\dot{\gamma} = (g^{\mathrm{opt}}_{\phi\phi})^{-1/2}\partial_\phi, \tag{45}$$

$$\ddot{\gamma} = (g^{\mathrm{opt}}_{rr})^{-1/2}\partial_r, \tag{46}$$

respectively. So, the geodesic curvature is simply

$$\kappa = g^{\mathrm{opt}}_{rr}(\nabla_{\dot{\gamma}}\dot{\gamma})^r\ddot{\gamma}^r, \tag{47}$$

where

$$(\nabla_{\dot{\gamma}}\dot{\gamma})^r = \Gamma^r_{\phi\phi}\dot{\gamma}^\phi\dot{\gamma}^\phi, \tag{48}$$

and

$$g^{\mathrm{opt}}_{\phi\phi,r} = \frac{2g^{\mathrm{opt}}_{\phi\phi}}{r}\left(1 - 4\pi\rho_0 r_0^2\left(1 - \frac{\ln(R+1)}{R}\right)\right). \tag{49}$$

With the additional factor $dt/d\phi = \sqrt{g^{\mathrm{opt}}_{\phi\phi}}$, the integrand of the line integral in Eq. (16) is

$$\kappa\frac{dt}{d\phi} = \frac{1}{r}\sqrt{\frac{g^{\mathrm{opt}}_{\phi\phi}}{g^{\mathrm{opt}}_{rr}}}\left(1 - 4\pi\rho_0 r_0^2\left(1 - \frac{\ln(R+1)}{R}\right)\right). \tag{50}$$

And taking the limit $r \to \infty$, we find

$$\lim_{r\to\infty}\kappa\frac{dt}{d\phi} = 1 - 8\pi\rho_0 r_0^2. \tag{51}$$

Finally from Eqs. (42) and (51), the deflection angle is

$$\delta(B) = 8\pi\rho_0 r_0^2\left(\pi - \frac{I_3}{B}\right) = \frac{16\pi\rho r_0^2}{B}\left(-\ln\frac{B}{2} + \sqrt{B^2-1}\arctan\sqrt{B^2-1}\right). \tag{52}$$

Here, $\delta(0) = 0$ and $\delta(\infty) = 8\pi^2\rho_0 r_0^2$. Note that the deflection at $B = \infty$ is nonvanishing. We will discuss this in Sec. VI.

F. Case (0, $\beta \geq 4$)

All the remaining cases are calculated in the same manner as the previous ones, so we will only present results from here on.

For this case, we have

$$\rho(R) = \frac{\rho_0}{(R+1)^\beta}, \tag{53}$$

$$m(R) = 4\pi\rho_0 r_0^3\left(\left(\frac{1}{\beta-3} - \frac{2}{\beta-2} + \frac{1}{\beta-1}\right) - \frac{1}{\beta-3}\frac{1}{(R+1)^{\beta-3}} + \frac{2}{\beta-2}\frac{1}{(R+1)^{\beta-2}} - \frac{1}{\beta-1}\frac{1}{(R+1)^{\beta-1}}\right), \tag{54}$$

$$\mathcal{K} = 8\pi\rho_0 r_0^2\left(-\frac{R}{(R+1)^\beta} - \frac{1}{\beta-3}\frac{1}{(R+1)^{\beta-1}} + \frac{2}{(\beta-3)(\beta-2)(\beta-1)}\sum_{i=2}^{\beta-1}\frac{i-1}{(R+1)^i}\right), \tag{55}$$

$$\delta(B)=\frac{8\pi\rho_0 r_0^2}{(\beta-1)(\beta-2)(\beta-3)}\left(\frac{4}{B}-2\frac{I_1^{\beta-1}}{B}+(\beta-4)(\beta-1)I_2^{\beta-1}-(\beta-2)(\beta-1)I_2^{\beta-2}\right). \tag{56}$$

One can check that $\delta(0)=\delta(\infty)=0$.

G. Case (0,3)

Here,

$$\rho(R)=\frac{\rho_0}{(R+1)^3}, \tag{57}$$

$$m(R)=4\pi\rho_0 r_0^3\left(\ln(R+1)+\frac{2}{R+1}-\frac{1}{2}\frac{1}{(R+1)^2}-\frac{3}{2}\right), \tag{58}$$

$$\delta(B)=8\pi\rho_0 r_0^2\left(\frac{1}{2}I_2^2-\frac{3}{2}I_2^1+\frac{I_3}{B}\right). \tag{59}$$

Similarly, $\delta(0)=\delta(\infty)=0$.

H. Case (0,2)

This density is of the type $\beta=2$, so the calculation is similar to the case (1,2). With the density and mass functions

$$\rho(R)=\frac{\rho_0}{(R+1)^2}, \tag{60}$$

$$m(R)=4\pi\rho_0 r_0^3\left(-2\ln(R+1)-\frac{1}{R+1}-\frac{1}{2}\frac{1}{(R+1)^2}+R+1\right), \tag{61}$$

the area integral in Eq. (16) gives

$$\delta_{\text{area}}(B)=8\pi\rho_0 r_0^2\left(I_2^1-2\frac{I_3}{B}\right). \tag{62}$$

For the line integral part, we calculate first the metric coefficients

$$e^{2A}\approx C^{-2}(R+1)^{8\pi\rho_0 r_0^2(1-2R^{-1})}, \tag{63}$$

$$e^{2B}\approx(1+8\pi\rho_0 r_0^2)-8\pi\rho_0 r_0^2\left(\frac{1}{R+1}-\frac{2\ln(R+1)}{R}\right). \tag{64}$$

Evaluating Eq. (4), we get

$$\kappa\frac{dt}{d\phi}=\frac{1}{r}\sqrt{\frac{g_{\phi\phi}^{\text{opt}}}{g_{rr}^{\text{opt}}}}\left(1-4\pi\rho_0 r_0^2\left(\frac{R-2}{R+1}+\frac{2\ln(R+1)}{R}\right)\right). \tag{65}$$

This shares the same limit in Eq. (51). Finally, we get the deflection angle from Eqs. (62) and (51),

$$\delta(B)=8\pi\rho_0 r_0^2\left(\pi-2\frac{I_3}{B}+I_2^1\right). \tag{66}$$

Just as the previous case (1,2), we have $\delta(0)=0$ and $\delta(\infty)=8\pi^2\rho_0 r_0^2$.

VI. DISCUSSION

The deflection angles computed from the energy density sequence (α,β) are well characterized by their $b\to 0$ and $b\to\infty$ limits. These limiting behaviors reflect the geometry of the optical manifold at the center and the asymptotic regions, respectively. The only two limiting behaviors are (1) a vanishing deflection angle corresponding to a locally flat (Euclidean) region, and (2) a nonzero deflection angle limit determined by a conical structure at the region. Table I gives a summary of the deflection angle limits.

Vanishing deflection at zero impact parameter in an asymptotically Euclidean spacetime is guaranteed when there are no singularities anywhere. By the angular symmetry of the metric, the geodesic light trajectory at $b=0$ (in the optical manifold) must be the straight line in flat space coincident with the x axis. Thus, the surface D in the central Eq. (16) is just the upper half-disk centered at C where S and O are at the vertices. With this surface, it is no surprise from the left-hand side of Eq. (16) that $\delta(0)=0$. While this argument may appear trivial at first, it is instructive to state it here because its conclusion is not obvious from the Gaussian curvature integral in Eq. (21). Moreover, the reasoning will not apply when there is a singularity at C.

TABLE I. Summary of deflection angle limits at zero and infinite impact parameter.

	$\beta=2$ m_∞ undefined, asymptotically conical, $\delta(\infty)=8\pi^2\rho_0 r_0^2$	$\beta=3$ m_∞ undefined, asymptotically Euclidean, $\delta(\infty)=0$	$\beta\geq 4$ m_∞ defined, asymptotically Euclidean, $\delta(\infty)=0$
$\alpha=0$, flat center, $\delta(0)=0$			Dehnen-type ($\beta=4$), Plummer-like ($\beta=5$)
$\alpha=1$, flat center, $\delta(0)=0$		NFW	Hernquist ($\beta=4$)
$\alpha=2$, conical center, $\delta(0)=8\pi^2\rho_0 r_0^2$	Singular isothermal sphere		Jaffe ($\beta=4$)

The central geometry of densities with $\alpha = 2$ approaches the singular isothermal sphere (SIS) geometry. The singular center prohibits the direct use of the upper-half disk when calculating the deflection angle at the zero impact parameter. The Gauss-Bonnet theorem cannot be applied to this surface because the boundary touches the singularity at the origin. One can only use a surface, like D, that approaches the half-disk. In fact, the Gaussian curvature integral approaches a nonzero value as $b \to 0$. This value is related to the central geometry of the optical manifold. We see here how the Gauss-Bonnet method highlights the role of topology in the contrasting central behavior of $\alpha = 0$, 1 and $\alpha = 2$ densities.

Gibbons and Werner [35] showed that the embedding of the low-density SIS optical manifold, with isotropic velocity dispersion σ^2, in flat $\mathbb{R}^3$ charted by (S, ϕ, z) is the cone

$$z = \sqrt{8\sigma^2}\frac{(1-\frac{9\sigma^2}{2})^{1/2}}{1-6\sigma^2}S. \tag{67}$$

In terms of ρ_0 and r_0, $\sigma^2 = 2\pi\rho_0 r_0^2$. A cone $z = kS$ has a deficit angle Δ of

$$\Delta = 2\pi\left(1-\sqrt{\frac{1}{k^2+1}}\right) \tag{68}$$

(derived in the Appendix). Up to first order in μ, the SIS deflection angle is

$$\delta_{\mathrm{SIS}} = \Delta/2 = 8\pi^2\rho_0 r_0^2. \tag{69}$$

That is, the constant SIS deflection angle is half the deficit angle of its conical optical manifold. From this point of view, deflection by SIS is entirely topological, i.e., due to the deficit angle of the conical manifold. We notice that this is the same value of the zero impact parameter limit of deflection by $\alpha = 2$ densities. This suggests that such deflections are also due to the conical center of the $\alpha = 2$ optical manifolds.

The infinite impact parameter behavior of deflection is more apparent to see. For asymptotically Euclidean spacetimes, it is clear from Eq. (21) that the integral must vanish as the lower bound of R approaches the upper bound. Meanwhile, $\beta = 2$ densities approach SIS distribution at large radial distances; thus the embedding in flat $\mathbb{R}^3$ of this region of the optical manifold is also approximately conical. As expected, we get a deflection angle of $\delta(\infty) = \Delta/2 = 8\pi^2\rho_0 r_0^2$, similar to the case of $\alpha = 2$ when $b = 0$.

Plots of deflection angles are shown in Fig. 2. The deflection by $\beta = 2$ densities always approach the angle $\Delta/2$ as the impact parameter grows large. Meanwhile, the deflection for $\beta = 3$ falls off considerably slower than $\beta \geq 4$ due to logarithmic terms plaguing the decay. We also note that since the density function of (0,5,1) behaves

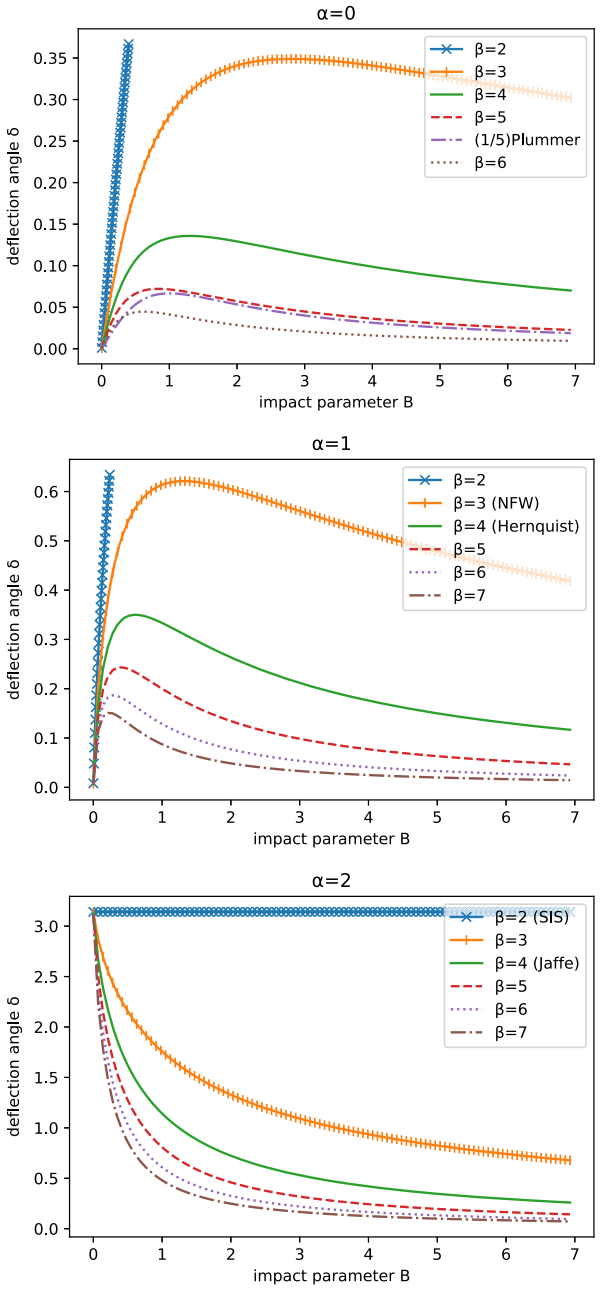

FIG. 2. Plots of deflection angles in factors of $8\pi\rho_0 r_0^2$ as a function of the scaled impact parameter $B = b/r_0$. The Plummer curve is scaled down by 1/5 to emphasize its resemblance to the (0,5,1) curve. All $\beta = 2$ deflections approach the angle $\Delta/2$ as $b \to \infty$, although these are not covered by the span of the plots.

comparable to the Plummer sphere $(0, 5, 1/2)$, the Plummer deflection (e.g., [35]) follows roughly the deflection curve of (0,5,1) given a suitable scale factor. Evans and Wilkinson [34] also proposed a mass distribution similar to Eq. (2) where it is the projected surface mass density that follows a two-power law. The corresponding actual (three-dimensional) density function of their surface density surely has a different form from Eq. (2), so similarities in deflection are only qualitative. For example, there seems

to be a similarity in the trend between the α of three-dimensional two-power densities and its two-dimensional $\alpha-1$ counterpart. This "one power less in α" similarity makes sense from the difference of the mass function in Eq. (10), for three-dimensional densities, from the total enclosed surface mass inside the circle $s=s'$: $M(s')=\int_0^{s'}\Sigma(s)2\pi s ds$, for surface mass densities. The former has r^2 in the integrand while the latter only has s—one power less than r^2.

Finally, we note that with other methods the calculations would have been more complicated with integrals appearing in impractical forms.

VII. CONCLUSIONS AND RECOMMENDATIONS

To summarize, using the Gauss-Bonnet technique, we have obtained new analytic expressions for the first-order deflection angle due to spherical two-power-law densities $(\alpha,\beta,1)$ in Eq. (2) for $\alpha=0,\ 1,\ 2$ and $\beta=2,3,4,\ldots$. These expressions are valid in the weak-field regime, $\mu=\rho_0 r_0^2\ll 1$, as well as arising from nonrelativistic matter. Our main results are presented in Eq. (27) for the case $(2,\beta\geq 4)$, Eq. (31) for (2,3), Eq. (35) for $(1,\beta\geq 4)$, Eq. (39) for (1,3) or the NFW, Eq. (52) for (1,2), Eq. (56) for $(0,\beta\geq 4)$, Eq. (59) for (0,3), and Eq. (66) for (0,2). Explicit forms are determined for the named densities: Hernquist in Eq. (36), NFW, and Jaffe in Eq. (28). Our calculated Hernquist and NFW deflections are consistent with the result of Keeton [32] and Bartelmann [33], respectively. Comparing our deflection with that of Evans and Wilkinson we also find good qualitative agreement. Our calculations demonstrate how the Gauss-Bonnet method can be more convenient for weakly deflecting spherical distributions compared to canonical methods, such as integration from $g(p^\mu,p^\mu)$ and the method of the thin lens approximation.

We have demonstrated that the Gibbons-Werner insight into the role played by topology in gravitational deflection extends to mass distributions beyond those that the authors initially considered, as is explicitly demonstrated in the $\alpha=0,\ 1$ and $\alpha=2$ densities. We have shown how the topological properties of the corresponding optical manifold immediately imply vanishing deflection for the former cases and finite deflection for the latter case in the limit of zero impact parameter. The central region of $\alpha=0,\ 1$ densities is flat (Euclidean), while that of $\alpha=2$ densities is conical. The topology-controlled behavior of the deflection also obtains in the $b\to\infty$ limit. At this limit, there is a finite deflection for $\beta=2$ densities and vanishing deflection for $\beta>2$ densities. This is due to the asymptotically conical optical manifold of the former and the asymptotically Euclidean optical manifold of the latter. At these conical regions, two-power densities are well approximated by the singular isothermal sphere distribution. Gibbons and Werner [35] previously noted that the constant deflection angle of the low-density singular isothermal sphere takes the value of half the deficit angle of its conical optical manifold, suggesting that the deflection is due to the conical angle defect. Here, we find the same to be true for the limiting cases of $\alpha=2$ and $\beta=2$. Outside the limiting behaviors of the deflection, however, we emphasize that geometrical details of the optical manifold do play the dominant role.

An immediate extension of this study is to find a general expression that includes noninteger values of α and β, which may provide a better fit with certain galactic densities. Such values complicate the form of the integrals and render invalid the analytic techniques used here. We seek to address these and related questions in future work.

ACKNOWLEDGMENTS

K. D. L. is grateful to Gary Gibbons for helpful conversations that shaped the writing of this paper. We also thank Reginald Bernardo and an anonymous referee for their helpful comments and careful reading of the manuscript. This research is supported by the University of the Philippines OVPAA through Grant No. OVPAA-BPhD-2016-13.

APPENDIX A: PARTIAL FRACTION DECOMPOSITION: DENOMINATOR WITH TWO DISTINCT ROOTS

We wish to find the coefficients A_i and B_j that satisfy

$$\frac{1}{(x-a)^p(x-b)^q}=\sum_{i=1}^{p}\frac{A_i}{(x-a)^i}+\sum_{j=1}^{q}\frac{B_j}{(x-b)^j},\tag{A1}$$

where p and q are positive integers. The partial fraction decomposition looks somehow similar to Laurent expansions. This suggests that the coefficients might be extracted from relevant Laurent series expansions. We start by appealing to this well-known Kronecker delta expression as an isolation tool,

$$\frac{1}{2\pi i}\oint_{C_a}\frac{dz}{(z-a)^n}=\delta_{1n},\tag{A2}$$

where C_a is a closed contour enclosing the singular point $z=a$. Suppose we want to find the coefficient A_k. To utilize Eq. (A2), we multiply both sides of Eq. (A1) with $(x-a)^{k-1}$, so that

$$\frac{1}{(x-a)^{p-k+1}(x-b)^q}=\sum_{i=-k+2}^{p-k+1}\frac{A_{i+k-1}}{(x-a)^i}+(x-a)^{k+1}\sum_{j=1}^{q}\frac{B_j}{(x-b)^j}.\tag{A3}$$

Integrating both sides of Eq. (A3) on the complex plane along the closed contour C_a, we find that on the right-hand

side only the $i = 1$ term survives on the first summation, as per relation (A2), while the second summation vanishes altogether because it is an analytic function on the domain enclosed by the contour. Thus,

$$A_k = \frac{1}{2\pi i}\oint_{C_a}\frac{1}{(x-a)^{p-k+1}(x-b)^q}dx. \tag{A4}$$

This is easily evaluated with the calculus of residues:

$$A_k = \frac{1}{(p-k)!}\left(\frac{\partial}{\partial a}\right)^{p-k}_{x=a}\frac{1}{(x-b)^q}, \tag{A5}$$

$$A_k = \binom{p+q-1-k}{q-1}\frac{(-1)^{p-k}}{(a-b)^{p+q-k}}. \tag{A6}$$

The coefficients B_j are obtained in the same manner:

$$B_k = \binom{p+q-1-k}{p-1}\frac{(-1)^{q-k}}{(b-a)^{p+q-k}}. \tag{A7}$$

APPENDIX B: EVALUATING THE I_i INTEGRALS

Only the integrals I_1 and I_3 are sketched here. I_2 is evaluated in the same manner as I_1 with some slight modifications.

1. I_1 and I_2

We use complex integration to evaluate the integral I_1. First, note that

$$I_1^q = \int_0^\pi \frac{\sin\phi d\phi}{(1+B\csc\phi)^q} = \Im\left[\int_0^\pi \frac{e^{i\phi}d\phi}{(1+B\csc\phi)^q}\right] =: \Im[\mathcal{I}]. \tag{B1}$$

We instead deal with the integral $\mathcal{I}$. However, the exponent of the denominator still complicates the evaluation. As a way out, we proceed as follows:

$$\begin{aligned}\mathcal{I} &= \frac{1}{B^q}\int_0^\pi \frac{e^{i\phi}d\phi}{(B^{-1}+\csc\phi)^q}\\ &= \frac{1}{B^q}\left(\int_0^\pi \frac{e^{i\phi}d\phi}{(a+\csc\phi)^q}\right)_{a=1/B}\\ &= \frac{1}{B^q}\frac{(-1)^{q-1}}{(q-1)!}\left(\frac{\partial}{\partial a}\right)^{q-1}_{a=1/B}\left(\int_0^\pi \frac{e^{i\phi}d\phi}{a+\csc\phi}\right).\end{aligned} \tag{B2}$$

Let the integral in the last line of Eq. (B2) be $\mathcal{J}$. The overall form of $\mathcal{J}$ suggests that the contour of the integral in the complex plane is a semicircular arc centered at $z = 0$ of unit modulus. Hence, we consider the integral

$$\mathcal{K} = \frac{1}{i}\oint_{\mathcal{C}}\frac{z^2-1}{az^2+2iz-a}dz, \tag{B3}$$

where $\mathcal{C} = \mathcal{C}_1 + \mathcal{C}_2$ is the contour traversed in the positive sense given by

$$\mathcal{C}_1:\ z(x) = x, x\in[-1,1], \tag{B4}$$

$$\mathcal{C}_2:\ z(\phi) = e^{i\phi}, \phi\in[0,\pi]. \tag{B5}$$

The simple poles are at

$$z_\pm = i\left(-\frac{1}{a}\pm\sqrt{\frac{1}{a^2}-1}\right). \tag{B6}$$

Notice that the poles are never inside the domain enclosed by the contour $\mathcal{C}$, so $\mathcal{K} = 0$, and

$$\mathcal{K} = \oint_{\mathcal{C}_1}(\cdots) + \oint_{\mathcal{C}_2}(\cdots) = 0. \tag{B7}$$

The $\mathcal{C}_2$-integral is already $\mathcal{J}$, so

$$\mathcal{J} = -\frac{1}{i}\int_{-1}^1 \frac{x^2-1}{ax^2+2ix-a}dx. \tag{B8}$$

We consider first the case $0 < a < 1$ where the poles are purely imaginary. Later on, we will argue that the answer we get here is the same as when $a > 1$ by invoking the uniqueness of analytic continuation of functions (we expect $\mathcal{J}$ to be a well-behaved function of a). Evaluating $\mathcal{J}$ will finally give I_1^q.

2. I_3

Here, we evaluate the integral I_3

$$I_3 = \int_0^\pi \sin\phi\ln(1+B\csc\phi)d\phi. \tag{B9}$$

Integrating by parts once, we proceed as

$$\begin{aligned}I_3 &= (-\cos\phi\ln(1+B\csc\phi))|_0^\pi - \int_0^\pi \frac{B\cot^2\phi}{B\csc\phi+1}d\phi\\ &= (\cdots)|_0^\pi - \frac{1}{B}\int_0^\pi \frac{B^2(\csc^2\phi-1)}{B\csc\phi+1}d\phi\\ &= (\cdots)|_0^\pi - \frac{1}{B}\int_0^\pi \frac{(B^2\csc^2\phi-1)+(1-B^2)}{B\csc\phi+1}d\phi\\ &= (\cdots)|_0^\pi - \frac{1}{B}\int_0^\pi (B\csc\phi-1)d\phi - \left(\frac{1-B^2}{B}\right)I_2^1\\ &= (\cdots)|_0^\pi + \ln(\csc\phi+\cot\phi)|_0^\pi + \frac{\pi}{B} - \left(\frac{1-B^2}{B}\right)I_2^1\\ &= \ln\left(\frac{\csc\phi+\cot\phi}{(B\csc\phi+1)^{\cos\phi}}\right)\Bigg|_0^\pi + \frac{\pi}{B} - \left(\frac{1-B^2}{B}\right)I_2^1\\ &= \pi B + 2\ln\frac{B}{2} - 2\sqrt{B^2-1}\arctan\sqrt{B^2-1}.\end{aligned} \tag{B10}$$

It should be noted that the logarithmic terms on the sixth line are undefined individually; only their difference has a finite limit.

APPENDIX C: DEFICIT ANGLE OF A CONE

The deficit angle of a cone is defined by its slope k. Consider the cone $z - kS = 0$ in flat $\mathbb{R}$ charted by cylindrical coordinates (S, ϕ, z). The induced metric on the cone is

$$ds^2_{\text{cone}} = dS^2 + S^2 d\phi^2 + d(kS)^2 \tag{C1}$$

$$= (k^2 + 1)(dS^2 + S^2 d\tilde{\phi}^2), \tag{C2}$$

where

$$\tilde{\phi} = \frac{\phi}{\sqrt{k^2 + 1}}. \tag{C3}$$

We see that the metric on the conical surface is conformal to the Euclidean metric, but with a reduced angular range: $\tilde{\phi} \in [0, 2\pi/\sqrt{k^2 + 1})$. Thus, the deficit angle is

$$\Delta = 2\pi\left(1 - \sqrt{\frac{1}{k^2 + 1}}\right) = \pi k^2 + \mathcal{O}(k^4). \tag{C4}$$

[1] P. Coles, in *Historical Development of Modern Cosmology* (University of Chicago Press, Chicago, Illinois, 2001), Vol. 252, p. 21.
[2] D. Kennefick, in *Einstein and the Changing Worldviews of Physics* (Springer, New York, 2012), pp. 201–232.
[3] D. E. Lebach, B. E. Corey, I. I. Shapiro, M. I. Ratner, J. C. Webber, A. E. E. Rogers, J. L. Davis, and T. A. Herring, Phys. Rev. Lett. **75**, 1439 (1995).
[4] R. Reyes, R. Mandelbaum, U. Seljak, T. Baldauf, J. E. Gunn, L. Lombriser, and R. E. Smith, Nature (London) **464**, 256 (2010).
[5] J. A. Tyson, F. Valdes, and R. Wenk, Astrophys. J. **349**, L1 (1990).
[6] R. B. Metcalf and P. Madau, Astrophys. J. **563**, 9 (2001).
[7] A. D. Rivero, C. Dvorkin, F.-Y. Cyr-Racine, J. Zavala, and M. Vogelsberger, Phys. Rev. D **98**, 103517 (2018).
[8] S. Birrer, T. Treu, C. Rusu, V. Bonvin, C. Fassnacht, J. Chan, A. Agnello, A. Shajib, G. C. Chen, M. Auger *et al.*, Mon. Not. R. Astron. Soc. **484**, 4726 (2019).
[9] C. B. Morrison, D. Klaes, J. L. van den Busch, P. Schneider, P. Simon, R. Nakajima, T. Erben, H. Hildebrandt, A. Grado, N. Napolitano *et al.*, Mon. Not. R. Astron. Soc. **465**, 1454 (2016).
[10] T. Abbott, F. Abdalla, A. Alarcon, J. Aleksić, S. Allam, S. Allen, A. Amara, J. Annis, J. Asorey, S. Avila *et al.*, Phys. Rev. D **98**, 043526 (2018).
[11] H. Diehl, T. Abbott, J. Annis, R. Armstrong, L. Baruah, A. Bermeo, G. Bernstein, E. Beynon, C. Bruderer, E. Buckley-Geer *et al.*, in *Observatory Operations: Strategies, Processes, and Systems V* (International Society for Optics and Photonics, Bellingham, Washington, 2014), Vol. 9149, p. 91490V, http://dx.doi.org/10.1117/12.2056982.
[12] W. Hu and T. Okamoto, Astrophys. J. **574**, 566 (2002).
[13] P. L. Kelly, J. M. Diego, S. Rodney, N. Kaiser, T. Broadhurst, A. Zitrin, T. Treu, P. G. Pérez-González, T. Morishita, M. Jauzac *et al.*, Nat. Astron. **2**, 334 (2018).
[14] C. Fian, E. Mediavilla, J. Jiménez-Vicente, J. Muñoz, and A. Hanslmeier, Astrophys. J. **869**, 132 (2018).
[15] B. Salmon, D. Coe, L. Bradley, M. Bradač, V. Strait, R. Paterno-Mahler, K.-H. Huang, P. A. Oesch, A. Zitrin, A. Acebron *et al.*, Astrophys. J. Lett. **864**, L22 (2018).
[16] A. Acebron, N. Cibirka, A. Zitrin, D. Coe, I. Agulli, K. Sharon, M. Bradač, B. Frye, R. C. Livermore, G. Mahler *et al.*, Astrophys. J. **858**, 42 (2018).
[17] C. Lamarche, A. Verma, A. Vishwas, G. Stacey, D. Brisbin, C. Ferkinhoff, T. Nikola, S. Higdon, J. Higdon, and M. Tecza, Astrophys. J. **867**, 140 (2018).
[18] J. A. Zavala, A. Montaña, D. H. Hughes, M. S. Yun, R. Ivison, E. Valiante, D. Wilner, J. Spilker, I. Aretxaga, S. Eales *et al.*, Nat. Astron. **2**, 56 (2018).
[19] R. Kayser and T. Schramm, Astron. Astrophys. **191**, 39 (1988).
[20] S. Warren and S. Dye, Astrophys. J. **590**, 673 (2003).
[21] L. Hernquist, Astrophys. J. **356**, 359 (1990).
[22] W. Dehnen, Mon. Not. R. Astron. Soc. **265**, 250 (1993).
[23] S. Tremaine, D. O. Richstone, Y.-I. Byun, A. Dressler, S. Faber, C. Grillmair, J. Kormendy, and T. R. Lauer, Astron. J. **107**, 634 (1994).
[24] H. Zhao, Mon. Not. R. Astron. Soc. **278**, 488 (1996).
[25] T. R. Lauer, S. Faber, C. R. Lynds, W. A. Baum, S. Ewald, E. J. Groth, J. J. Hester, J. A. Holtzman, J. Kristian, R. M. Light *et al.*, Astron. J. **103**, 703 (1992).
[26] T. R. Lauer, S. Faber, E. J. Groth, E. J. Shaya, B. Campbell, A. Code, D. G. Currie, W. A. Baum, S. Ewald, J. J. Hester *et al.*, Astron. J. **106**, 1436 (1993).
[27] S. Faber, S. Tremaine, E. A. Ajhar, Y.-I. Byun, A. Dressler, K. Gebhardt, C. Grillmair, J. Kormendy, T. R. Lauer, and D. Richstone, Astron. J. **114**, 1771 (1997).
[28] J. F. Navarro, C. S. Frenk, and S. D. M. White, Mon. Not. R. Astron. Soc. **275**, 720 (1995).
[29] W. Jaffe, Mon. Not. R. Astron. Soc. **202**, 995 (1983).
[30] K.-H. Chae, V. K. Khersonsky, and D. A. Turnshek, Astrophys. J. **506**, 80 (1998).
[31] K.-H. Chae, Astrophys. J. **568**, 500 (2002).
[32] C. R. Keeton, arXiv:astro-ph/0102341.
[33] M. Bartelmann, Astron. Astrophys. **313**, 697 (1996).

[34] N. Evans and M. Wilkinson, Mon. Not. R. Astron. Soc. **296**, 800 (1998).
[35] G. W. Gibbons and M. C. Werner, Classical Quantum Gravity **25**, 235009 (2008).
[36] K. Jusufi, Int. J. Geom. Methods Mod. Phys. **14**, 1750179 (2017).
[37] K. Jusufi and A. Övgün, Phys. Rev. D **97**, 024042 (2018).
[38] G. Crisnejo and E. Gallo, Phys. Rev. D **97**, 124016 (2018).
[39] Y. Rosenfeld, Mol. Phys. **86**, 637 (1995).
[40] L. H. Ryder, Eur. J. Phys. **12**, 15 (1991).
[41] L. Yang, Y.-Q. Ma, and X.-G. Li, Physica (Amsterdam) **456B**, 359 (2015).
[42] M. Bañados, C. Teitelboim, and J. Zanelli, Phys. Rev. Lett. **72**, 957 (1994).
[43] C. van de Bruck and C. Longden, Galaxies **7**, 39 (2019).
[44] A. Övgün, Universe **5**, 115 (2019).
[45] W. Klingenberg, *A Course in Differential Geometry* (Springer Science & Business Media, New York, 2013), Vol. 51.
[46] R. Wald, *General Relativity* (University of Chicago Press, Chicago, 2010).
[47] B. Schutz, *A First Course in General Relativity* (Cambridge University Press, Cambridge, England, 2009).
[48] A. Ishihara, Y. Suzuki, T. Ono, T. Kitamura, and H. Asada, Phys. Rev. D **94**, 084015 (2016).
[49] H. Arakida, Gen. Relativ. Gravit. **50**, 48 (2018).
[50] S. Mollerach and E. Roulet, *Gravitational Lensing and Microlensing* (World Scientific, Singapore, 2002).
[51] P. Schneider, J. Ehlers, and E. Falco, *Gravitational Lenses*, Astronomy and Astrophysics Library (Springer, Berlin Heidelberg, 2013).